Journal of Advanced Joining Processes 1 (2020) 100005

Contents lists available at ScienceDirect

Journal of Advanced Joining Processes

journal homepage: www.elsevier.com/locate/jajp

Process monitoring of ultrasonic metal welding of battery tabs using external sensor data

I. Balz[a,*], E. Abi Raad[b], E. Rosenthal[c], R. Lohoff[c], A. Schiebahn[a], U. Reisgen[a], M. Vorländer[b]

[a] RWTH Aachen University, ISF – Welding and Joining Institute, Pontstr. 49, 52062 Aachen, Germany
[b] RWTH Aachen University, Institute of Technical Acoustics, Kopernikusstraße 5, 52074 Aachen, Germany
[c] Forschungszentrum Jülich, ZEA-1 – Central Institute of Engineering, Electronics and Analytics, 52425 Jülich, Germany

ARTICLE INFO

Keywords:
Ultrasonic metal welding
Battery manufacturing
Process monitoring
Sensor
Quality control

ABSTRACT

Ultrasonic metal welding (USMW) is a common used manufacturing technology for cell, module or pack assembly of Lithium-ion battery systems of pouch type. Since every single joint can affect the efficiency and safety of the entire battery system, quality fluctuations of the joint are one of the greatest challenges. Despite its industrial spread in battery manufacturing, USMW has a large number of influencing variables that may affect the bond quality but cannot be detected 100% failsafe with existing monitoring methods.

Therefore the aim of this paper is to investigate the oscillation behavior of the tools and the joining members during USMW under different manufacturing conditions by monitoring external sensor data of structure-borne sound.

In this paper typical manufacturing conditions in battery tab welding such as rolling direction and amplitude are set in order to study their effects on joint quality and the corresponding sensor signals. Therefore two laser vibrometers record the tool vibrations of the anvil and horn during the process. Occasionally, high-speed image capturing is also used to investigate the mechanism of process influences by studying the in-situ oscillation behavior of horn, anvil and the workpieces during USMW process. The sensor data analysis is correlated to thermal measurements and to the results of T-peel tensile testing and microstructural characterization of the bond interface to understand the effects of process influences during the welding process and its resulting joint quality.

Based on the results, new insights for enhancing the process monitoring of USMW in Lithium-ion battery manufacturing are provided from identified sensor signals, that are correlating with the joint quality respectively different manufacturing conditions.

Introduction

Ultrasonic metal welding (USMW) is a solid state welding process using high frequency oscillations by applying a static clamping force. Since bonding is formed in solid state, ultrasonic metal welding provides good weldability for filigree, multilayer and dissimilar metal joints (Lee, 2013). Thus the process is widely used in battery manufacturing, like for example in cell and module assembly of battery pouch cells (Lee, 2013; Wodara and Adam, 2004; Lee et al., 2014). Since every single joint can affect the efficiency, safety and lifetime of the entire battery pack, a reproducible joint quality is essential. However, one of the biggest challenges in ultrasonic metal welding is the large number of influencing variables that may affect the joint quality.

Fluctuations of manufacturing conditions in battery welding can be caused both by joining members and by the welding system. Depending on type and severity of these influencing variables they lead to more or less fluctuations in bond quality.

As an example short cycle times in the USMW can lead to heating of the horn (Zäh et al., 2002). Due to thermal elongation, the oscillator system becomes detuned and the amplitude decreases (Zäh et al., 2002). Fluctuations in amplitude have a decisive influence on the achievable joint strength because the amplitude determines the intensity of friction between the joining members, especially having in mind of the high frequencies (Wodara and Adam, 2004; Zäh et al., 2002; Al-Sarraf and Lucas, 2012). With increasing amplitude, the friction work (Siddiq and Ghassemieh, 2009; Koellhoffer et al., 2011) increases and usually also the joint strength (Satpathy et al., 2015; Mohan Raj et al., 2018;

* Corresponding author.
E-mail address: balz@isf.rwth-aachen.de (I. Balz).

https://doi.org/10.1016/j.jajp.2020.100005
Received 20 November 2019; Received in revised form 28 January 2020; Accepted 28 January 2020

Satpathy and Sahoo, 2017). However, exceeding a maximum amplitude can also cause excessive alternating stresses within the joining members (Adam, 1999), especially if relative movement between the tools and joining members occurs.

Since bond formation occurs close to the surface of the joining members, even small changes in surface conditions can have a considerable influence on joint quality. Both the technical surface (roughness, waviness, coating, etc.) as well as the natural surface (dust, grease, oxides, etc.) must be taken into account. A too high surface roughness is assumed to hinder the relative movement between the joining members and the degradation of asperities, respectively, (Harthoorn, 1978; Satpathy and Sahoo, 2016). Whereas according to (Wodara and Adam, 2004) a too low surface roughness also leads to a decrease in joint strength. Although further research is needed on this topic, it can be summarized that the roughness and waviness determine the contact surface or the local surface pressure between the joining members as well as between them and the tools and thus have a significant influence on bond formation mechanisms.

In addition to the large number of influencing variables on joint quality, the USMW process is lacking in monitoring methods. As common industry standard random destructive peel and shear tensile tests are carried out to evaluate the joint quality in USMW. However, in such a fluctuating process like USMW, a sampling test is in principle to be critically assessed as short-term disturbances may not be detected. The simple monitoring of the welding parameters and their statistical evaluation as well as the process control via the limit value monitoring of parameters are currently state of the art in industrial series application (Greitmann et al., 2003). The majority of researchers agree that external sensor data are required to monitor the USMW process, as they correlate more sensitively with process fluctuations than conventional machine data (Lee, 2013; Lu et al., 2016; Lee et al., 2015; Balz et al., 2019; Sasaki et al., 2013). Exemplified by antiresonances, De Vries (2004) showed that electrical generator signals (e.g., electrical impedance) do not represent the complex nature of occurring welding mechanisms and are therefore insufficient for process monitoring. He concludes that direct measurements closer to the actual weld are necessary for process monitoring.

In general, in-situ measurement during USMW as a highly dynamic process with very small oscillation amplitudes is still challenging. Therefore, there are only few studies in which the in-situ oscillation behavior of horn, anvil and the workpieces has been investigated:

Laser Doppler Vibrometer (LDV) measurement of single spot (Balle et al., 2009) or multiple spots (Lu et al., 2016) was used to determine the oscillations during USMW. Lu et al. (2016) used a Photonic Doppler Velocimetry (PVD) to study the relative motion between the horn, aluminum foils and anvil and in order to define a welding stage model. Here it must be noted that the measurement includes only three spots (horn, upper foil, lower foil) simultaneously and therefore had to be repeated for the anvil. In addition, Abi Raad et al. (2019) investigated the applicability of acoustic emission and vibration analysis to find features to describe the different stages of a USMW process by looking at data recorded by two laser vibrometers and a microphone. Initial correlations between the vibrations of the tools and welding temperatures, penetration depth and bond strength could be found and were linked to the different stages of welding. However, some elements of vibrational behavior and the airborne sound could not be properly explained yet.

High-speed camera technique is another possibility to analyze the oscillations with Digital Image Correlation (DIC). Lee (2013), Lee et al. (2015), Sasaki et al. (2013) and Balz et al. (2019) used this method to study the interactions between the workpieces and the tools during welding. In contrast to laser vibrometry, a time-synchronized acquisition of the horn, anvil as well of the workpieces is possible depending on the chosen observation area of the camera. Disadvantages are the lower resolution (2 µm–3 µm) and the limited frame rates (100,000 fps) compared to vibrometry.

The above-mentioned studies have shown initial results on relative motions of the tools and the joining members during USMW. However, there is still a lack of characteristic features from sensor signals, which introduce the prospective to apply monitoring criteria for USMW.

In order to remain competitive to other joining technologies for battery manufacturing such as laser beam welding and resistance welding and to exploit the process benefits of USMW, the mechanisms of process influences on USMW require a better understanding. On the other hand, a detection of primary influencing variables based on sensor features is necessary in order to guarantee a reproducible bond quality. Therefore the aim of this paper is to investigate the vibrational behavior during USMW under different manufacturing conditions by monitoring external sensor data of structure-borne sound.

Experimental setup

Ultrasonic welding setup

For the investigation, similar lap welds made of copper (CW-008A, R240) sheets with 0.8 mm thickness were prepared by USMW. The dimensions of the samples were 45 mm × 125 mm. As shown in Fig. 1, two different orientations of the rolling direction (RD) were investigated: oscillation direction (OD) in rolling direction (sample identifier: IRD) and transverse to rolling direction (sample identifier: TRD).

A Schunk Sonosytems LS-C longitudinal welding system with a 20 kHz operating frequency and a maximum power of 4 kW was used for welding. The maximum vibration amplitude under no-load conditions was 28 µm (≙110%). The dimension of the horn surface was 8 mm × 8 mm knurled with 0,8 mm base side, 0,3 mm height and 90° apex angle. In order to reduce inconsistency in weld quality, energy-controlled mode was used in the present study. The range of optimal welding parameters was set by preliminary experimental tests for standard configuration (≙TRD). The highest joint quality (high strength, slight scattering) was achieved at a clamping force of 2.250 N ($p_{cylinder}$ = 4,5 bar), an oscillation amplitude of 26 µm (≙100%) and a weld energy of 1.800 Ws (average welding time ~867 ms).

In order to investigate the effects of amplitude changes on bond formation and on sensor signals the amplitude was varied systematically from 90% to 110% while keeping a constant clamping force of about 2250 N applied by a pneumatic cylinder. Besides that the welding time to reach the set energy was recorded by the ultrasonic welding machine. To investigate the influence of rolling direction, the welding parameters were kept constant [clamping force: 2.250 N, oscillation amplitude: 26 µm (≙100%), weld energy: 1.800 Ws] and only the orientation of rolling direction was changed.

Metrological test setup for process monitoring

In this study two Compact Laser Vibrometer “CLV-2534” from Polytec were used to record the vibrations of the horn and the anvil along the welding direction during welding. Occasionally, a high-speed camera “Fastcam Mini AX100” from Photron with telescope lens was arranged perpendicular to OD (x-axis) to record oscillation behavior of the entire mechanical system (including the workpieces) as shown in Fig. 2. The data from all those external sensors were synchronously recorded by a data acquisition system from National Instruments (NI) and a measuring computer with a LabView user interface. The chosen sampling rate for laser vibrometer was 250.000 Hz and for high-speed camera 127.500 Hz. Both LDV use a 633 nm wavelength helium-neon-source. The locations of the laser spots are illustrated in Fig. 2(a). Despite the small spot size (~110 µm), measurement errors due to process emissions, such as metal particles and dust, increasingly dominated at the measurement position (2), close to the weld zone. Therefore, the majority of the experimental measurements were carried out in the middle of the horn, position (1).

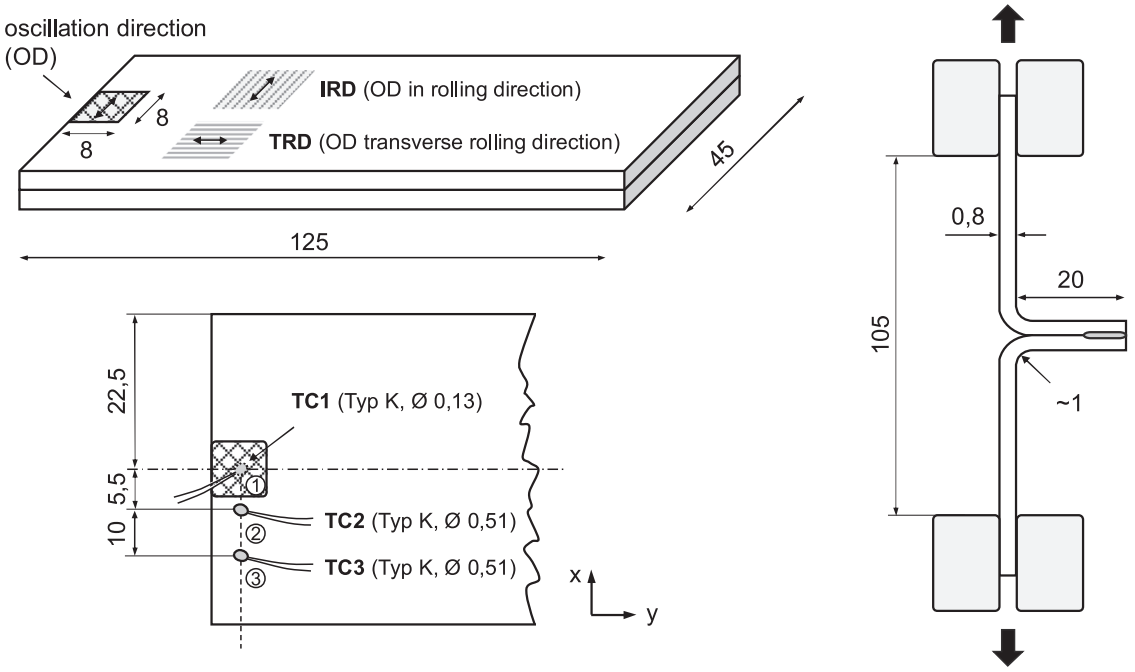

Fig. 1. Geometric specifications of weld specimen.

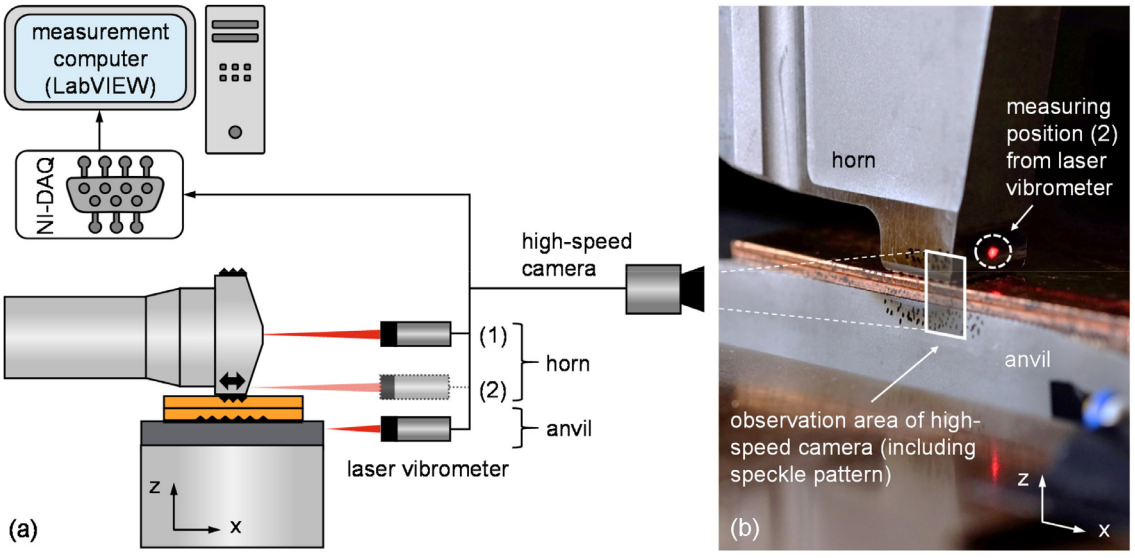

Fig. 2. (a) Schematic illustration of measurement setup and (b) zoomed in view showing a typical measuring configuration during tab welding.

The high-speed camera was placed perpendicular to OD. To compute a dense optical flow from the recorded image-sequences using the Gunnar Farnebäck algorithm (Farnebäck, 2003), speckle pattern were created on the tool and workpiece end surfaces, which were adjusted flush to each other. The observation area (image size: 64 px × 128 px) includes the knurled edge of the horn tip, the upper (US) and lower (LS) specimen and the knurled edge of the anvil, see Fig. 2(b). To illuminate the observation area, two high power LED modules VD7000 with a luminous flux of 7280 lm were installed and adjusted. The noise in recording, caused by the camera setup, the image noise and its processing, can be calculated from the computed displacements of the fixed sheet determined in preliminary investigations. The calculated measuring error corresponds to a displacement between 1,7 µm and 3,1 µm, depending on oscillation amplitude. Especially small amplitudes (< 5 µm) are superimposed by the image noise and lead to larger relative measuring errors. In Matlab®, the optical flow vectors of each image were transferred into a 3-dimensional matrix to analyze the time course of the displacements. For each object (horn, metal sheets and anvil) a representative object area consisting of four rows was chosen and the mean value of all x-components was calculated. From this, the displacement of the individual objects was determined as a function of image unit or weld time.

In order to estimate the temperature development during bond formation, two K-type thermocouples (Ø 0,51 mm) were ultrasonically welded at the top of the upper specimen at 10 mm (TC2) and 17 mm distance (TC3) from the horn. A third K-type thermocouple (Ø 0,13 mm) was placed between the two sheets in the middle of the welding zone (TC1), as shown in Fig. 1. As the integrated thermocouples may have an influence on bond formation, the temperature measurements were carried out in addition to the main experiments.

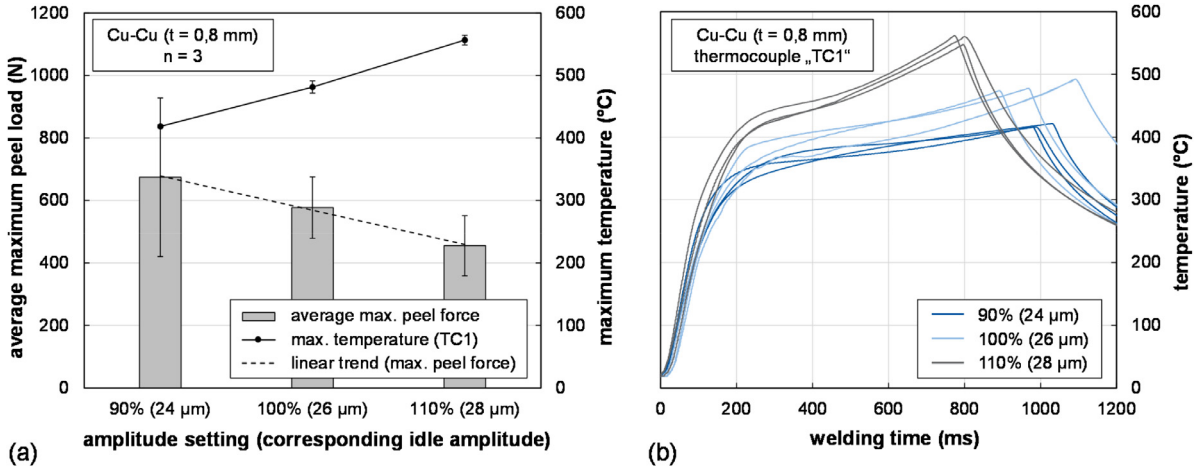

Fig. 3. (a) average maximum peel load and maximum temperature (TC1) as a function of amplitude, (b) temperature development during welding at different amplitude settings.

Evaluation of bond

T-peel tensile testing based on DIN EN 14,270 as shown in Fig. 1 was performed to evaluate weld quality and to observe the fractured surface. After welding, the sheets were bent by 90° in two directions to allow the specimen to be clamped. A load was then applied to peel the weld sample with a displacement rate of 10 mm/min. The maximum T-peel load from the load-displacement curve and the failure mode was recorded. In order to analyze the welded area (microbonds), the fracture surfaces of the peeled samples were measured with scanning electron microscope (SEM) "Leo 1530". Additional weld samples were cross-sectioned parallel to OD, polished and applied to a light surface etching using an aqueous solutions of nitric acid for further optical micrographs.

Results

Effect of oscillation amplitude on weld formation and sensor data

As seen before, the amplitude and the associated frictional heat are considerable influencing variables in USMW. The average maximum peel load and the corresponding maximum temperatures for three different amplitude settings are shown in Fig. 3(a). Here it can be seen that with increasing amplitude setting the peel forces decrease linearly by 32,5%, where the scattering is decreasing. The maximum temperature within the welding zone (TC1) shows a contrary trend: Increasing the amplitude by 4 µm causes a temperature increase of up to 33%. The corresponding temperature development curves as a function of welding time can be seen in Fig. 3(b). For each amplitude setting three measurements were taken. The basic trend along the temperature curves at different amplitude settings are similar: After a strong, almost linear temperature rise at the beginning of the welding process (< 200 ms), the temperature rise slows down and increases again towards the end of the welding process, where the temperature reaches its maximum. A higher amplitude causes a stronger temperature rise after reaching the first temperature plateau (~200 ms), which can also be seen in the decrease of welding time in the present case (energy-controlled mode). Interfacial failure occurs mainly in samples with 90% (24 µm) amplitude. With increasing amplitude the failure mode changes and partial interfacial separation with tear can be observed. Samples with 110% (28 µm) show cohesive failure with nugget pull-out fracture.

In order to understand the effects of the amplitude on bond formation, the cross-sectional microstructure of welded specimen with different amplitude settings is shown in Fig. 4.

Smaller amplitudes (a) show some microbonds and a clearly visible border line due to less surface fitting, which indicates a low plastic deformation. This explains the higher scattering in joint strengths, because small differences in the surface topography of the sheets has a greater influence on the size and number of microcontacts and –bonds in comparison to a larger plastic deformation. With increasing amplitude (b) the fraction and size of local bonded regions increases. Moreover, the microstructure of the heat affected zone changes to coarse grains in case of higher amplitudes (c).

Fig. 5(a) shows the output power curves for the different amplitude settings as a function of welding time. The different amplitude settings can be clearly distinguished by the curves. On the one hand, welds with a higher amplitude require a correspondingly higher power output. On the other hand, the power peak at the beginning of the welding process (~100 ms) is less pronounced with a decreasing amplitude. The same applies for the renewed power increase at the end of the welding process, which can be observed at amplitude settings of 110%.

Clear differences can also be seen in the vertical displacement of the horn recorded by the machine, see Fig. 5(b). In the initial phase (< 200 ms), the curves nearly superimpose each other. Here, the different amplitudes do not seem to have an influence on the vertical displacement of the horn. Only after reaching the theoretical maximum penetration depth of the horn (~300 µm), the curves diversify. The highest values of the vertical displacement of the horn are found at the highest amplitude settings. The difference of the maximum penetration depth between welding samples with 90% and 110% is about 240 µm, which confirms, in good agreement with the previous observations, the significant effect of the amplitude on plastic deformation.

In order to display the effect of the amplitude setting on bond formation, Fig. 6 shows the peak envelope of the amplitude of the horn (a) and the upper sheet (b) calculated from the high-speed images. The plotted profiles represent two typical welds for each amplitude setting. For this, the raw signals were filtered with a bandpass between 15 kHz and 25 kHz. Then the envelope of the peaks was extracted and finally the moving average smoothing method was used to smooth the resulting data.

Despite the fact that the amplitude of the horn in contact area to the upper sheet ("actual amplitude") is significantly damped (~ −40%) compared to the theoretically expected amplitudes ("set amplitude", see in legend of the charts), the mean oscillation amplitudes of the horn in contact area vary in good approximation with the amplitudes step settings. With smaller amplitudes, an approximately constant course is recognizable after ramping-up, whereas with 110% amplitude a higher

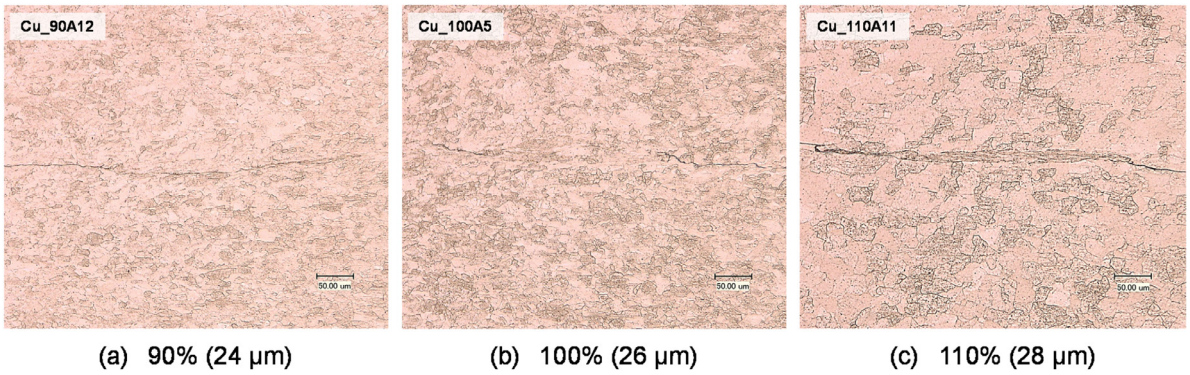

Fig. 4. Micrographs of cross-sectioned CW-008A welded specimen with different amplitude settings: (a) 90%, (b) 100%, (c) 110%.

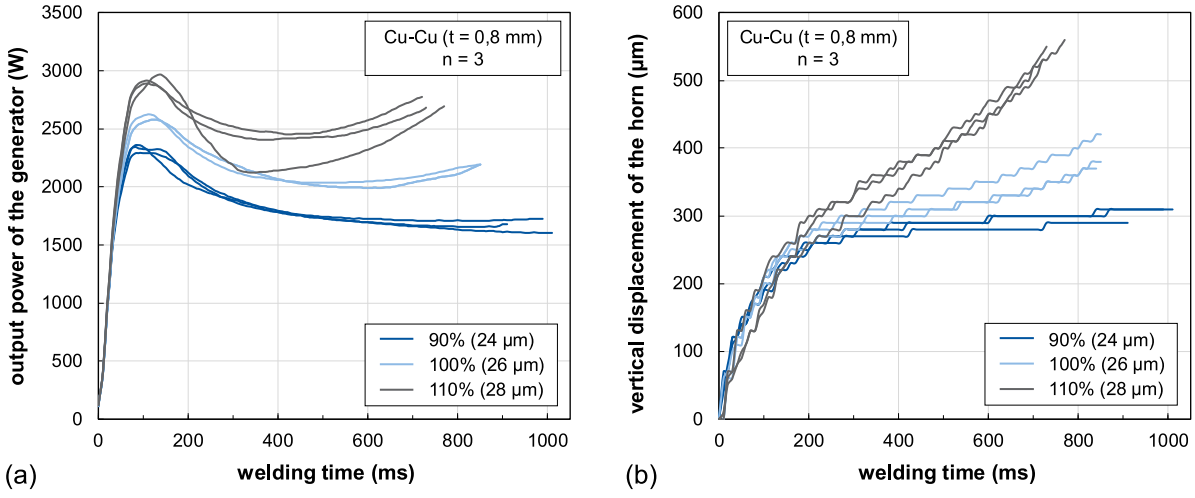

Fig. 5. Effect of amplitude on machine signals: (a) output power curve and (b) vertical displacement of the horn as a function of welding time.

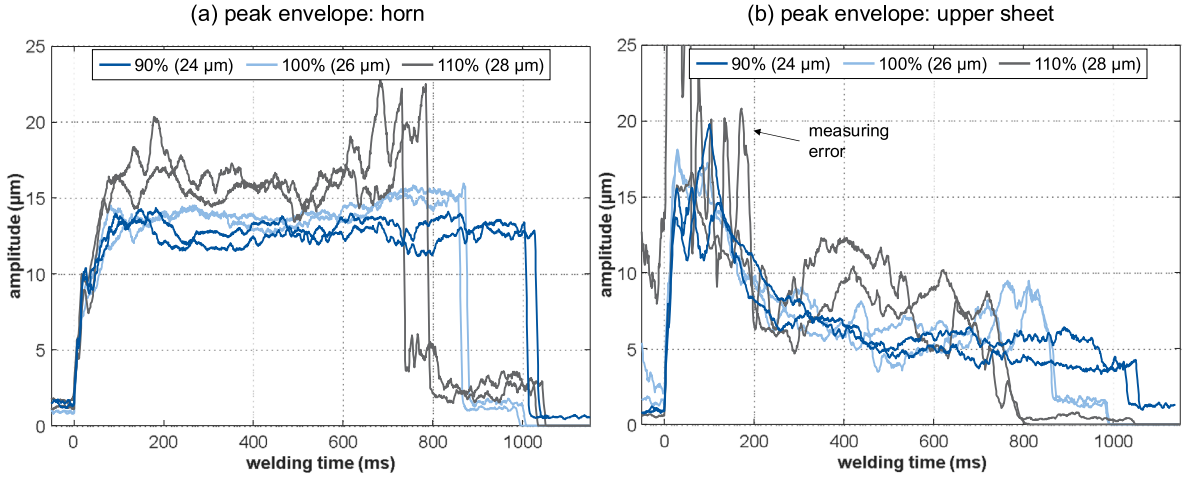

Fig. 6. Effect of amplitude setting on real oscillation amplitude of the horn in contact area (a) and the upper sheet (b) calculated from the high-speed images (bandpass: 15 kHz–25 kHz).

oscillation amplitude is recognizable at the beginning as well as at the end of the welding process.

Although high-speed image capturing provides interesting insights into the interactions within the welding zone, Fig. 6(b) also illustrates the fact that these measurements are error-prone and therefore had to be repeated frequently. The figure also shows that during the ramp-up phase, the amplitude profiles of the upper sheet are approximately superimposed and in addition higher than those of the horn. After this ramp-up phase (>200 ms) wider variations are apparent for the different amplitude settings: At 110% amplitude the upper sheet is more excited to oscillate, whereas at 100% and 90% the amplitude profiles tend to stagnate at a lower amplitude level.

Since the determined amplitudes of the lower sheets and the anvil are generally smaller than 5 µm and the signals therefore have larger noise components. Therefore detailed consideration of these components has been dispensed in the present paper. With regard to the relative it can

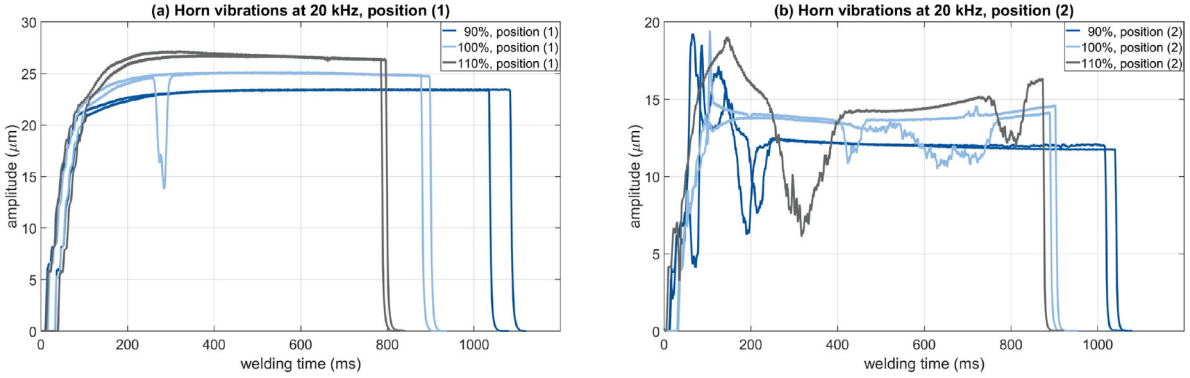

Fig. 7. Horn vibrations at 90%, 100% and 110%, measured at (a) position 1 and (b) position 2.

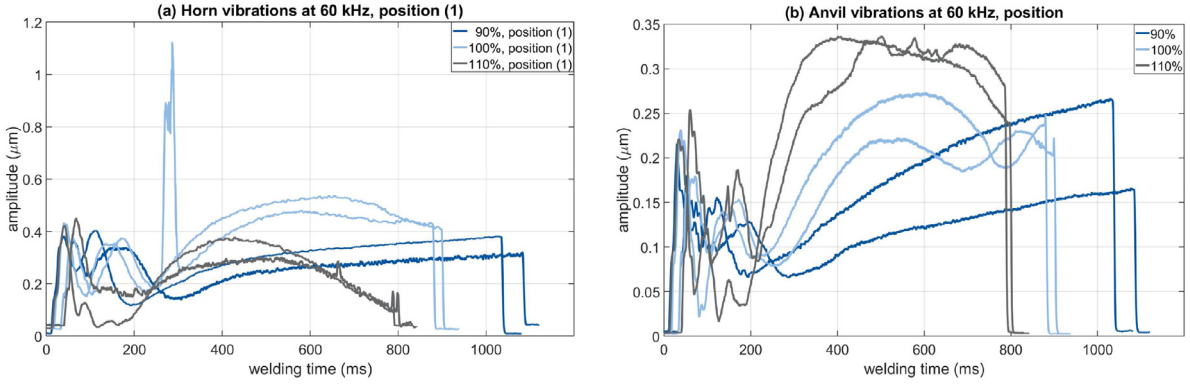

Fig. 8. Horn (position 1) and Anvil vibrations at 90%, 100% and 110% at 60 kHz.

be said movements in general that the beginning of the welding process (< 200 ms) is characterized by an overall high relative movement between the sheets but also between the horn and the upper sheet. After 200 ms, the relative movement between the sheets drops strongly and increasing slippage occurs in the contact areas with the tools. The higher the amplitude setting, the greater the overall relative movements at the beginning and at the end of the welding process. This means that more energy is transferred into the system, which can also be seen in the peaks of the output power of the generator. In the samples with 110% amplitude, the horn also seems to couple better to the upper sheet due to the larger temperature rise at the beginning of the welding process. As a result, the horn is more damped. As a result between 300 ms and 600 ms there is mainly relative movement between the sheets. It is also interesting to note that as the amplitude setting increases, the slippage on the anvil decreases and the relative movement takes place mainly at the horn. Since the sheets experience a lower softening at smaller amplitudes, a higher excitation of the anvil can also be expected at the end of the welding process.

Figs. 7 and 8: Horn (position 1) and Anvil vibrations at 90%, 100% and 110% at 60 kHz and Fig. 9 show the displacement of the horn and anvil during welding, both at the welding frequency of 20 kHz and at some of its harmonics, for amplitudes settings 90%, 100% and 110%, and at positions (1) and (2). The displacement was calculated by integrating the velocity of the vibrations during welding, and then filtering that data into 10 kHz frequency bands centered around the frequencies of interest. Only the 20 kHz and 60 kHz frequencies are shown, because they are the most interesting and show the most striking differences between the cases.

As can be seen in Fig. 7, the magnitude of the vibrations at 110% is larger than at 100%, which itself has amplitudes larger than at 90%, both at position (1) and position (2). This was expected, and is also in accordance with the results from the high-speed camera data. The results from position (2) are closer to the results from the high-speed camera than the results from position (1). The difference comes from the fact that the camera data gives results that are much closer to position 2. Position 1 also shows less fluctuations than the camera data. This is due to the fact that position 1 is farther from the welding zone than the camera data, and so is less affected by the welding process.

Fig. 8(a), the horn vibrations at position (1) at 60 kHz, shows clear differences for the different amplitude settings. The horn vibrations for 110% first have a strong increase, between 200 ms and 400 ms, and then a strong decrease, which lasts until the end of the welding process. The 100% vibrations have a similar increase between 200 ms and 400 ms. Then, they keep increasing but with a decreasing slope until reaching a maximum around 600 ms, before decreasing at a slower rate than the 110%. As for the vibrations at 90%, they keep increasing at a steady rate starting 200 ms, and only reach their maximum at the end of the welding process. In Fig. 8(b), the anvil vibrations at 60 kHz, the vibrations for the 90%, 100% and 110% cases behave similarly to their horn counterparts: the 90% curves keep increasing from 200 ms to the end of the process, the 110% curves increase rapidly between 200 ms and 400 ms and then decreases until the end of the welding process, and the 100% increase until a bit before 600 ms.

Fig. 9 shows anvil vibrations at 20 kHz and 40 kHz. At 20 kHz and 40 kHz, the anvil vibrations are largest for 90% welds, and smallest for 110% welds. At 20 kHz, most welds have a slight decrease in amplitude after a maximum around 200 ms, with the decrease being faster with higher welding amplitudes. At 40 kHz, the curves reach a maximum around 200 ms, then decrease as the welding process progresses. Here too, the higher the amplitude of the weld, the steeper the decline. The 90% case is even almost constant towards the end of the welding process, compared to the 100% and 110% cases.

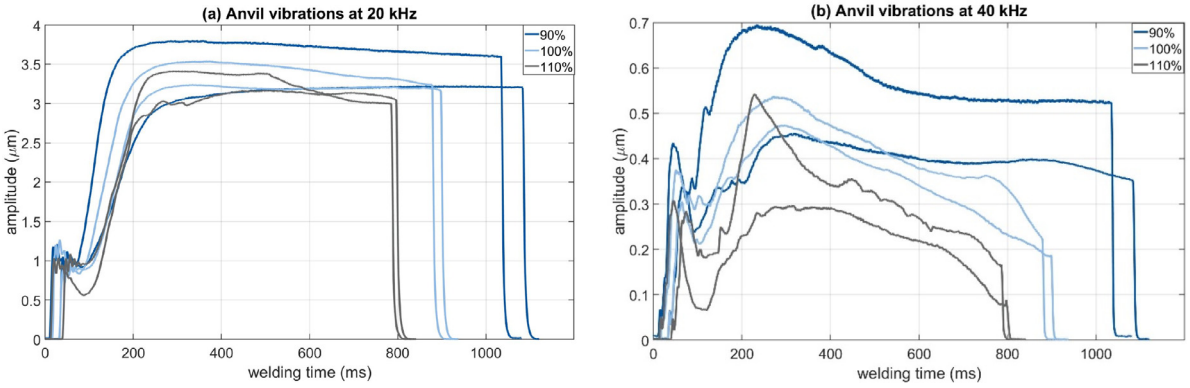

Fig. 9. Anvil vibrations at 90%, 100% and 110% at 20 kHz and 40 kHz.

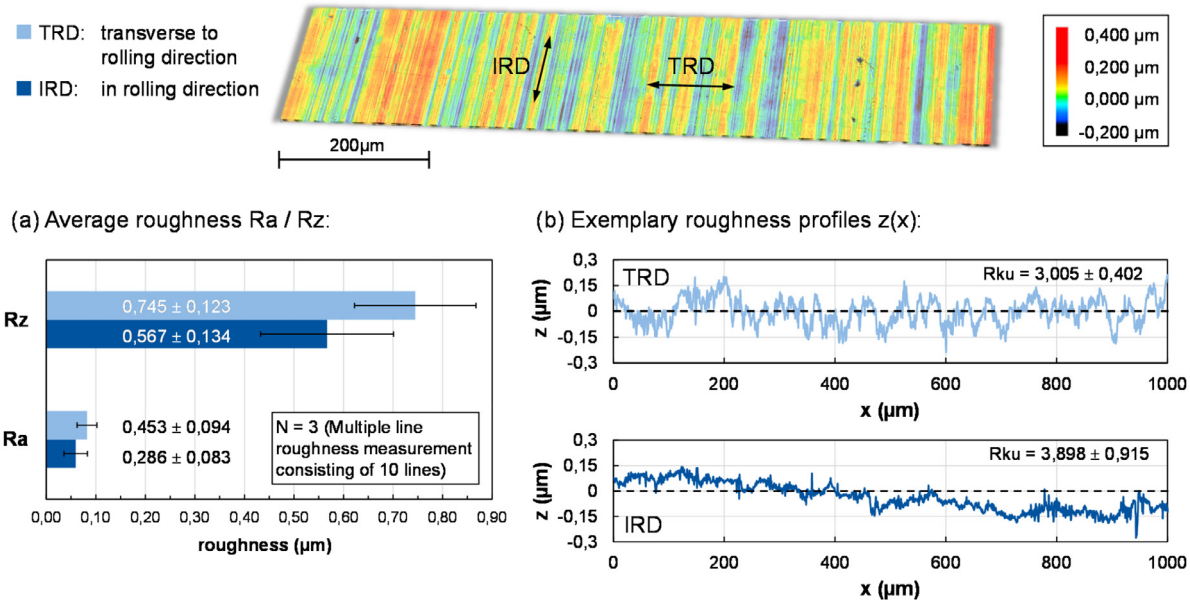

Fig. 10. Roughness measurements with 3D-laser confocal microscope transverse or in rolling direction: (a) average multiple line roughness Ra/Rz and (b) exemplary roughness profiles.

Effect of rolling direction on weld formation and sensor data

In addition to the machine parameters, the joining members and their surface properties may also affect the bond quality in battery manufacturing. A significantly measurable difference in the joint strength can be seen as a function of the orientation of the rolling direction. For this reason the multiple line roughness in and transverse to the rolling direction was determined with 3D-laser confocal microscope “VK-X1050” (Keyence) at 50x magnification to characterize the tab surfaces before the welding process. The top of Fig. 10 shows an exemplary, three-dimensionally measured tab surface with markings in (IRD) and transverse (TRD) to the rolling direction.

In order to quantify the direction-dependent texture of the surface, 10 roughness measurement lines were determined for each orientation, see exemplary roughness profiles in Fig. 10(b). From these measurement lines the average roughness Ra and Rz were calculated, see Fig. 10(a).

In case of TRD the roughness is higher compared to IRD. Expressed in values the mean roughness Ra is 0,453 µm (TRD) and 0,286 µm (IRD) and the mean roughness depth Rz is 0,745 µm (TRD) and 0,567 µm (IRD). Furthermore, Kurtosis Rku was determined, see Fig. 10(b): based on the measured values, it can be derived that the amplitude density curve of TRD is normally distributed, whereas IRD features statistically less pronounced profile peaks or profile valleys.

Fig. 11 shows the individual maximum peel loads of TRD and IRD weld samples with the resulting welding times. On average, the peel loads of TRD are about 88% higher than of IRD. In contrast, the resulting welding times do not differ significantly.

Looking at the characteristic fracture surfaces in the bottom of Fig. 11, noticeable differences can be seen. In both sample types the alignment of the elongated micro bonds runs in the same direction as the oscillation (OD). However, the fracture surface of TRD shows larger plastically deformed micro bonds in comparison to IRD. As already seen, plastic deformation within the welding zone in general correlates with the joint strength. This is also the case in the present situation.

Fig. 12(a) shows the output power curves for the different orientations of the rolling direction as a function of welding time. Here, in contrast to the amplitude settings, the curves cannot be delimited from each other. Minor differences can be seen in the vertical displacement of the horn, see Fig. 12(b). In good agreement with the previous observations and the assumption that plastic deformation is higher for TRD, the vertical displacement of the horn is on average slightly higher for TRD than for IRD welding samples. Since the curves show slight

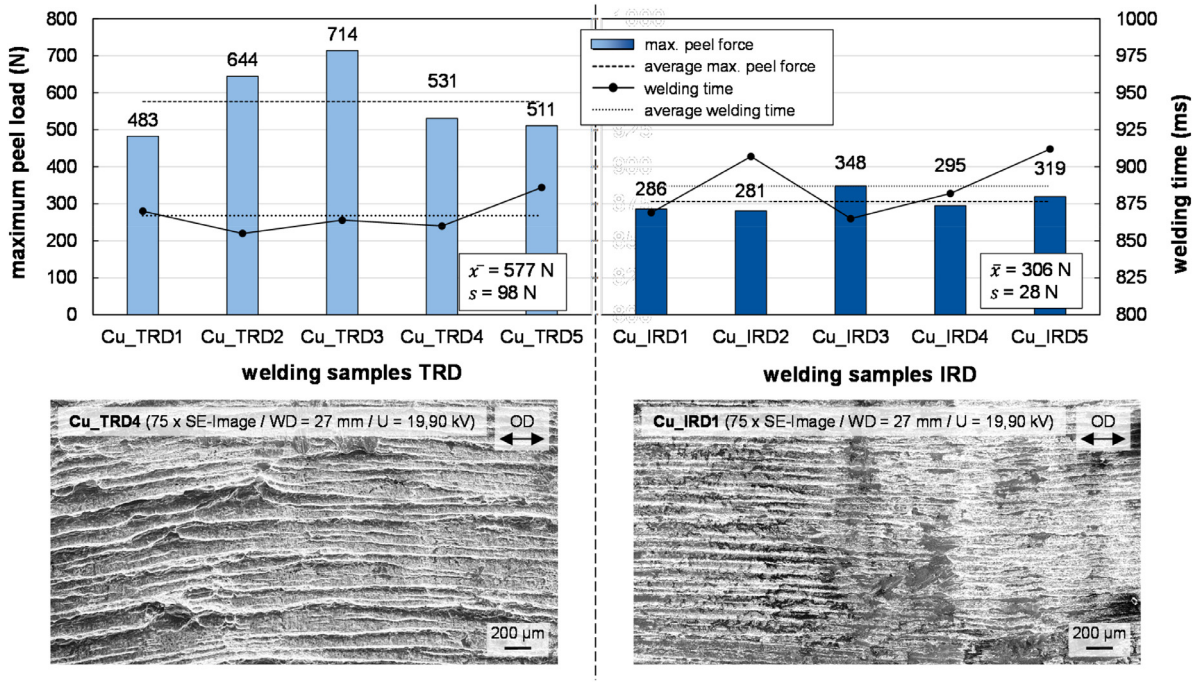

Fig. 11. Maximum peel loads and characteristic fracture surfaces (SEM) of individual welding samples with oscillation direction transverse rolling direction (left) or in rolling direction (right).

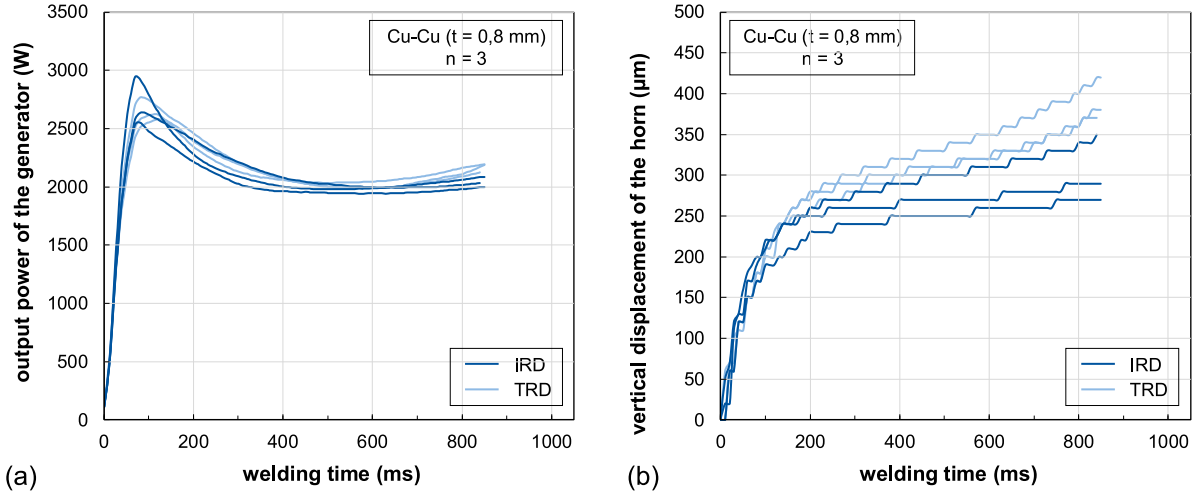

Fig. 12. Effect of rolling direction on machine signals: (a) output power curve and (b) vertical displacement of the horn as a function of welding time.

differences in the course, this machine signal is less suitable for reliably distinguishing the sample types from each other.

Fig. 13 shows the peak envelope of the amplitude of the horn (a) and the upper sheet (b) calculated from the high-speed images. The plotted profiles represent two typical welds for each rolling direction. In contrast to the influence of the amplitude setting, the amplitude values of the horn (Fig. 13(a)) are approximately equal, whereby a small increase in the final stage of the welding process can be seen in the amplitude profiles for TRD welding samples.

The different amplitude profiles (TRD and IRD) of the upper sheet are also almost identical, see Fig. 13(b). For TRD welding samples, an amplitude increase can be observed at the end of the welding process again. Since amplitude values of the horn and of the upper sheet rise equally, the relative movement between the horn and the upper sheet remains comparable between TRD and IRD welding samples.

Fig. 14 shows the horn vibrations at 20 kHz and 60 kHz, for IRD at position 1 and TRD at both position 1 and 2. Due to the higher error rates, no further recording of IRD at position 2 was done. At 20 kHz, the vibrations TRD at position (2) are in accordance with the results from the high-speed camera: the horn vibrates with a constant amplitude at an amplitude of 15 µm. As for TRD and IRD at position 1, they are also in accordance with the results of the high-speed camera: in both figures, the vibrations of IRD and TRD overlap almost perfectly. However, unlike the high-speed data, there is no increase in the vibration amplitude towards the end of the welding process neither the TRD nor the IRD. The main difference between position (1) and position (2) is the difference in amplitude, from 15 µm at point (2) to 25 µm at point (1). The vibrations at 60 kHz for IRD and TRD are similar at position (1), and smaller than the vibrations measured at position (2).

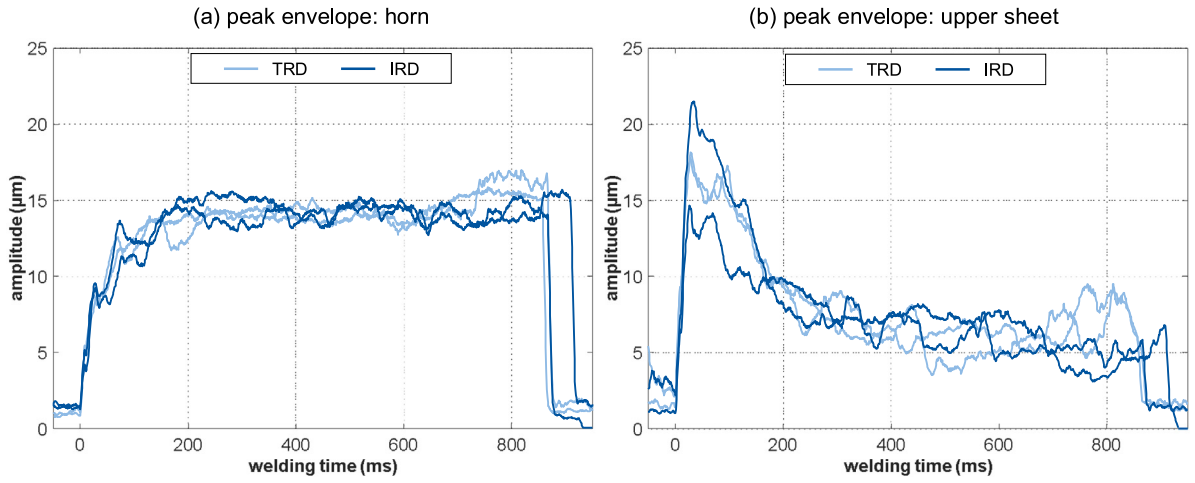

Fig. 13. Effect of rolling direction on real oscillation amplitude of the horn in contact area (a) and the upper sheet (b) calculated from the high-speed images (bandpass: 15 kHz–25 kHz).

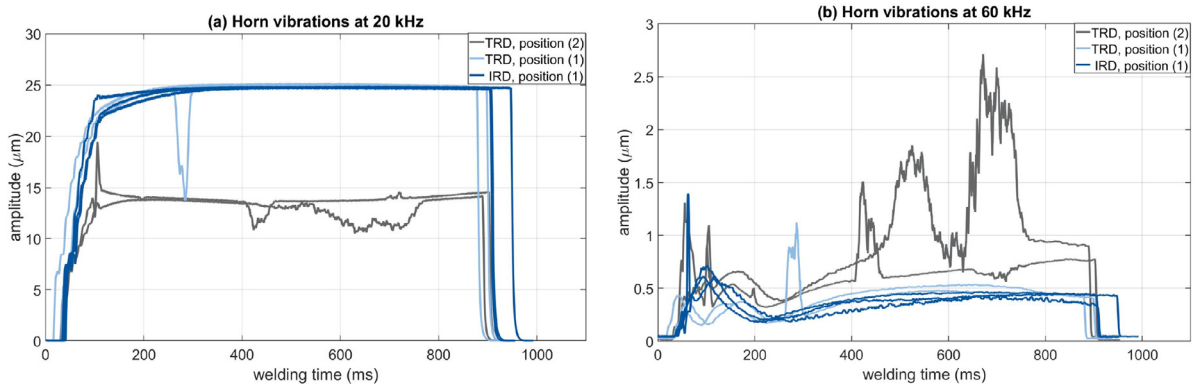

Fig. 14. Horn vibrations at (a) 20 kHz and (b) 60 kHz for TRD and IRD.

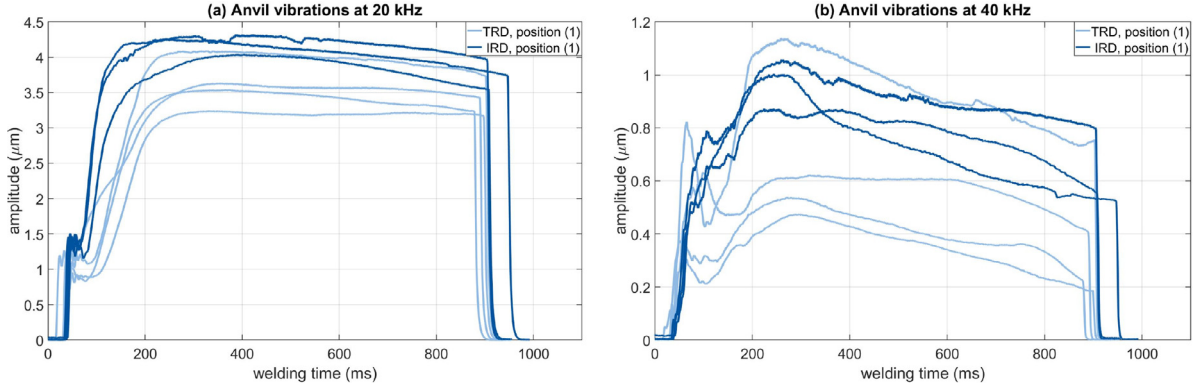

Fig. 15. Anvil vibrations at (a) 20 kHz and (b) 40 kHz.

The anvil vibrations at 20 kHz, 40 kHz and 60 kHz are shown in Figs. 15 and 16. Here, we see that the vibrations of the IRD are almost always higher than the vibrations of the TRD, for 20 kHz, 40 kHz and 60 kHz. The only TRD sample to have vibrations of a similar amplitude to the IRD vibrations is the TRD sample with the weakest strength: 482,7 N, compared to the 530,6 N, 644,5 N and 713,9 N of the others. This strength is still higher than the IRD samples (285,8 N, 280,7 N and 348.4 N), though even for the IRD samples, the strongest weld is the one with the smallest vibrations. At 20 kHz, the TRD and IRD samples have similar overall shapes: they reach a maximum early on, and stay relatively constant. The biggest difference comes from how fast they reach that maximum: the IRD curves reach their maximum in a total time of around 150 ms, while the TRD curves take about 200 ms to reach their maximum. At 40 kHz, the vibrations are characterized by an increase until a maximum is reached around 300 ms, followed by a decrease, with the weaker welds having the highest maximum. At 60 kHz, the vibrations are characterized by a minimum somewhere between 100 ms and 200 ms, followed by an increase that continues until the end of the welding process for the IRD samples, and that reaches a maximum around 600 ms for the TRD samples. After that maximum, most of the TRD samples have a decrease.

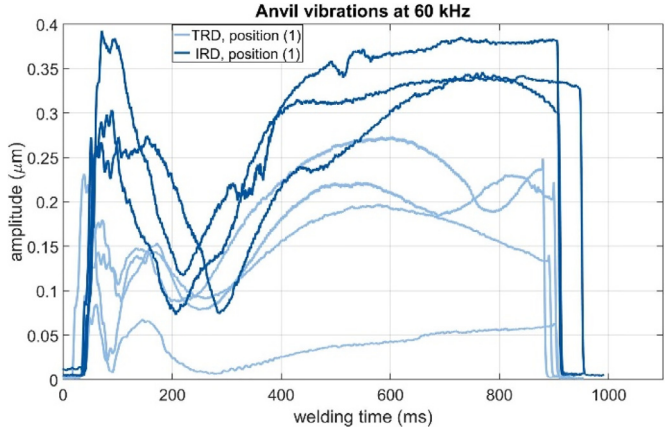

Fig. 16. Anvil vibrations at 60 kHz.

Discussion

Our Studies have shown that even small changes in the amplitude of vibration of the horn - within a few micrometers - have a significant impact on the temperatures and joint strength achieved during welding. The amplitude of vibration determines the frictional heat generated during the process, which itself determines the temperatures reached within the welding area. With the increase of temperature (in this case, up to ~400 °C) the yield strength decreases and material softening can be monitored along with a microstructural change (grain coarsening). According to literature values, the recrystallization temperature of copper is between 425 °C and 650 °C, depending on its deformation (Kupferinstitut, 2019). When welding at 110% amplitude, the temperature reaches this range shortly after the start. The results of the microsections as well as the vertical displacement curves of the horn confirm the assumption that a softening as a result of a grain growth caused by a recrystallization occurs during these welds. These effects can favor plastic deformation in the specimens.

On one hand, plastic deformation enables a shortening of the distance between the specimen on an atomic scale and thereby the formation of the joint. On the other hand, plastic deformation is necessary to ensure a coupling of the upper sheet and the horn. During the beginning of the USMW process (~ < 100 ms) the upper sheet oscillates with a higher oscillation amplitude than imposed by the horn. This is suspected to be caused by the lower inertia of the upper sheet and the missing coupling to the horn and the lower sheet at this initial stage. The resulting relative movement between the horn and the upper sheet is therefore higher at high amplitude settings (110%) than when using lower amplitude settings. As the excitation amplitude increases, the relative movement in the entire tribological system (on all contact areas) also increases. Accordingly, there is more friction and thus a higher temperature rise for welds with higher amplitude settings. A higher temperature rise can favor the penetration of the knurled pattern of the horn into the upper sheet, which leads to a better coupling between the horn and the upper sheet and thereby to a more efficient transfer of the oscillation energy into the upper specimen. This results in a larger relative movement between both sheets, which can be indicated for example by the lower power level of the generator between 300 ms and 600 ms at highest amplitude settings. If the temperature rises above the critical temperature (see specimen with 110%) due to occurring friction or deformation processes, the strength of the upper sheet is increasingly reduced. At the same time, the joint strength decreases. Finally, the strength of the upper specimen is not sufficient anymore to transfer the excitation force of the horn and a relative movement (slip) between the horn and the upper sheet increases towards the end of the process. Similar to the beginning of the process (coupling stage), this results in a temperature rise towards the end of the welding process, which is more pronounced with a higher amplitude setting. It is assumed that a strongly increasing slip of the horn towards the end of the process is an indication of an excessive softening of the upper sheet and therefore a decrease of the joint strength is to be expected. Further examinations are necessary to prove this hypothesis.

Based on the power and penetration curves of the system, the different amplitude settings can be distinguished from one another. Changes in amplitude caused by production fluctuations can certainly be smaller. Therefore, it is necessary to verify whether system data is sufficient for monitoring.

From the laser measurements, we can first note that the laser data at the horn, position (2) and at 20 kHz and the camera results are in agreement. The amplitudes and shapes of the signal are similar.

In addition, the data at the horn, position (1) is also similar to the data from position (2), but with larger vibrations. Then, we can note that differences between welding processes done at 110%, 100% and 90% amplitude setting are mostly seen in the behavior of the anvil. At 20 kHz, the welding frequency, the vibrations at 90% are larger than at 110%. This indicates a lower material softening at lower amplitudes. The anvil vibrations are also more even throughout the welding process at 90%. This is also seen at 40 kHz.

Looking at the evolution of the temperature and of anvil vibrations at 20 kHz, 40 kHz and 60 kHz, we can see that, as the temperature gets higher, the amplitude of vibrations decreases. Welds done with 110% amplitude show the fastest increase in temperature, especially towards the end of the welding process. At around 200 ms, the anvil vibrations see their maximum at 20 kHz and 40 kHz and their minimum at 60 kHz. This is also an inflection point in the temperature curves of the welds. After that, the temperature at 90%, 100% and 110% increase, but with a higher slope for the higher welding amplitude setting. The faster the temperature increase, the faster the amplitude of anvil vibrations decreases at the same time. These results corroborate the analysis done based on the high-speed camera recordings.

Furthermore, the results of the tests showed that the USMW process is very sensitive to surface conditions, such as rolling direction in this case. A change in the orientation of the rolling direction can have a significant impact on the joint strength, but cannot be reliably detected using data from the welding system. USMW is a near-surface process. Therefore, it is plausible that even the smallest changes in the surface topography can affect the occurring friction and deformation processes. Because temperature measurements by thermocouples within the welding area would have distorted the impact of the surface, it was not possible to measure temperature differences due to friction. However, analysis of the fractured surface allows for the conclusion that specimen with a transverse rolling direction experience a greater plastic deformation within the welding area. A greater plastic deformation results in a higher joint strength in accordance to the resulting peeling forces. A possible reason for this finding is the line-type profile peaks and valleys. In TRD specimens, these are transverse to the oscillation and can therefore be more easily removed and leveled by occurring shear forces. Such deformation processes can also contribute to heating the specimen and softening them. The evaluation of the recordings of the high-speed camera provides indications of a softening effect. Similarly to experiments examining the influence of higher oscillation amplitudes, a small rising oscillation amplitude of the horn can be seen towards the end of the welding process. In contrast to the thesis of Satpathy and Sahoo (2016), the high-speed measurements prove that the surface topography does not have an impact on the relative movement between both sheets. A higher roughness therefore does not necessarily hinder the relative movement between both sheets.

The laser data shows that the difference between TRD and IRD is best seen in the anvil vibrations, rather than the horn vibrations. The vibrations of the TRD samples are, on average, smaller than those of the IRD samples: at 20 kHz, the initial slope is more pronounced in the IRD samples, and at 40 kHz and 60 kHz, the amplitudes of vibrations are larger for the IRD samples. The fact that the anvil vibrations are smaller

in the case of the TRD samples can indicate that more energy is being transferred to the welding area and converted into, among other things, plastic deformation, as discussed previously. This plastic deformation benefits the formation of microwelds, and leads to a stronger bond. We can note, however, than even a weak TRD weld, which has vibrations of amplitudes similar to those of IRD welds, is still stronger than IRD welds. The decrease in anvil vibrations could also come from the increased softening of the copper sheets with the progress of the welding process. As the welding progresses and the temperature increases, the ductility of the copper sheets increases and leads to less energy being transferred to the anvil from the horn.

Conclusion

This paper investigates the behavior of the horn and anvil during USMW of battery tabs under different manufacturing conditions, such as different welding amplitude settings (90%, 100% and 110%) and rolling directions (TRD and IRD). To do that, it pools together data from many different sensors: temperature measurements, machine signals such as power curves and vertical displacement of the horn, high-speed camera imaging and LDV to measure the vibrations of the horn, upper sheet and anvil, peel load measurements to characterize the strength of the welds, and light- and electron-optical microscopy to evaluate the quality of the bond.

The results have confirmed that the USMW process is a sensitive welding process characterized by many influencing variables. The internal machine signals can occasionally identify process changes, but they are not reliable signal features for process monitoring in battery manufacturing.

The high-speed images in combination with the temperature measurements provide interesting insights into the thermo-mechanical mechanisms of the entire mechanical system and are very useful for a better understanding of the process. They have shown that influencing variables can affect the frictional behavior and thus the temperature development. Especially at the beginning of the welding process frictional heat dominates and influences the level of softening and plastic deformation of the sheets. In addition, the results of the influence of rolling direction have shown that the amount of plastic deformation is also determined by the surface characteristics of the sheets.

A minimum degree of joining temperatures and plastic deformation are required for a high joint quality. On the other hand, excessive temperatures or plastic deformation can reduce the strength again.

An external monitoring of the tools seems to be a suitable option for future process monitoring. In particular, the higher harmonic signals of the horn and anvil are sensitive to occurring changes due to influencing variables. However, welds can be better distinguished by looking at the anvil vibrations during welding. Furthermore the monitoring of the anvil seems to be more suitable due to its lower susceptibility (error-rate). Especially since the results have shown that the horn does not behave as a rigid body and the measuring position therefore strongly influences the measurement result.

Since, USMW process is a sensitive welding process, further investigations and data analyses will have to be carried in order to identify signal features that are as generally valid as possible.

Declaration of Competing Interest

The authors declare that they have no known competing financial interests or personal relationships that could have appeared to influence the work reported in this paper.

Acknowledgment

The authors would like to thank the European Regional Development Fund (ERDF) for the support of the research work under grant number EFRE-0800612. For the sponsorship and the support, we wish to express our sincere gratitude. We would also like thank the German Research Foundation DFG (RE2755/52-1). Furthermore we thank Dr. rer. nat. H. Glückler, Central Institute of Engineering, Electronics and Analytics (ZEA-1), Forschungszentrum Jülich, Jülich, Germany, for the fruitful discussion and excellent cooperation.

References

Abi Raad, E, Balz, I., Reisgen, U., Vorländer, M., 2019. Investigation of the applicability of acoustic emission and vibration analysis to describe the thermo-mechanical mechanism during ultrasonic metal welding. In: Proceedings of the 23rd International Congress on Acoustics, Integrating 4th EAA Euregio 2018. Deutsche Gesellschaft für Akustik (DEGA e.V.), Aachen, pp. 4700–4707.

Adam, T.: Ultraschallschweißen ausgewählter Aluminiumlegierungen mit erhöhter Festigkeit. Dissertation. Otto-von-Guericke-Universität, Magdeburg, 1999

Al-Sarraf, Z., Lucas, M., 2012. A study of weld quality in ultrasonic spot welding of similar and dissimilar metals. In: Proceedings of the International Conference on Modern Practice in Stress and Vibration Analysis, Journal of Physics, 382. IOP Publishing Ltd., Glasgow, pp. 012013/1–6.

Balle, F., Wagner, G., Eifler, D., 2009. Charakterisierung des ultraschallschweißprozesses durch hochauflösende laser-Doppler-vibrometrie. InFocus Magazin für Opt. Messsyst. 1.

Balz, I., Rosenthal, E., Reimer, A., Turiaux, M., Schiebahn, A., Reisgen, U., 2019. Analysis of the thermo-mechanical mechanism during ultrasonic welding of battery tabs using high-speed image capturing. Weld. World doi:10.1007/s40194-019-00788-z.

Farnebäck, G., 2003. Two-Frame motion estimation based on polynomial expansion. Image analysis. In: Proceedings of the 13th Scandinavian Conference, SCIA: 2749. Springer, Halmstad.

Greitmann, M.J., Adam, T., Holzweißig, H.G., Stroh, D., Wagner, G., Wiesner, P., Züst, R., 2003. Gegenwärtiger stand und zukunftsaussichten der sonderschweißverfahren - ultraschallschweißen. Schweißen Schneid. 55 (6), 306–314.

Harthoorn, J.L.: Ultrasonic Metal Welding. Dissertation. Technische Hogeschool Eindhoven, Eindhoven, 1978

Koellhoffer, S., Gillespie, J.W., Advani, S.G., Bogetti, T.A., 2011. Role of friction on the thermal development in ultrasonically consolidated aluminum foils and composites. J. Mater. Process. Technol. 211 (11), 1864–1877.

Kupferinstitut, D., 2019. Wärmebehandlung von kupferwerkstoffen. [Online]. Tabelle 39. [abgerufen am: 31.10.2019]. Verfügbar unter: https://www.kupferinstitut.de/de/werkstoffe/verarbeitung/waermebehandlung.html.

Lee, S.S., Shao, C., Kim, T.H., Hu, S.J., Kannatey-Asibu, E., Cai, W.W., Spicer, J.P., Abell, J.A., 2014. Characterization of ultrasonic metal welding by correlating online sensor signals with weld attributes. Trans. ASME J. Manuf. Sci. Eng. 136 (5), 51019.

Lee, S.S., Kim, T.H., Hu, S.J., Cai, W.W., Abell, J.A., 2015. Analysis of weld formation in multilayer ultrasonic metal welding using high-speed images. Trans. ASME J. Manuf. Sci. Eng. 137 (3), 031016/1–8.

Lee, S.: Process and Quality Characterization for Ultrasonic Welding of Lithium-Ion Batteries. Dissertation. University of Michigan, Michigan, 2013

Lu, Y., Song, H., Taber, G.A., Foster, D.R., Daehn, G.S., Zhang, W., 2016. In-situ measurement of relative motion during ultrasonic spot welding of aluminum alloy using photonic Doppler velocimetry. J. Mater. Process. Technol. 231, 431–440.

Mohan Raj, N., Kumaraswamidhas, L.A., Nalajam, K.P., Arungalai Vendan, S., 2018. Studies on electro mechanical aspects in ultrasonically welded Al/Cu joints. Trans. Indian Inst. Met. 71 (1), 107–116.

Sasaki, T., Watanabe, T., Hosokawa, Y., Yanagisawa, A., 2013. Analysis for relative motion in ultrasonic welding of aluminium sheet. Sci. Technol. Weld. Join. 18 (1), 19–24.

Satpathy, M.P., Sahoo, S.K., 2016. Microstructural and mechanical performance of ultrasonic spot welded Al–Cu joints for various surface conditions. J. Manuf. Process. 22, 108–114.

Satpathy, M.P., Sahoo, S.K., 2017. Parametric analysis on plastic deformation of materials during ultrasonic spot welding with different anvil geometries. Int. J. Manuf. Technol. Manag. 31 (4), 344–361.

Satpathy, M.P., Moharana, B.R., Dewangan, S., Sahoo, S.K., 2015. Modeling and optimization of ultrasonic metal welding on dissimilar sheets using fuzzy based genetic algorithm approach. Eng. Sci. Technol. 18 (4), 634–647.

Siddiq, A., Ghassemieh, E., 2009. Theoretical and FE analysis of ultrasonic welding of aluminum alloy 3003. Trans. ASME J. Manuf. Sci. Eng. 131 (4), 041007/1–11.

de Vries, E. Mechanics and Mechanisms of Ultrasonic Metal Welding. Dissertation. Ohio State University, Columbus, 2004

Wodara, J., Adam, T., 2004. Ultraschallfügen und -trennen. Band 1 der grundlagen der fügetechnik. Fachbuchreihe Schweißtechnik, 151. DVS Verlag, Düsseldorf ISBN 3-87155-212-7.

Zäh, M.F., Mosandl, T., Schlickenrieder, K., 2002. Ultraschall-metallschweißen. Steigerung der prozesssicherheit für das ultraschall-metallschweißen. Werkstattstechnik 92 (9), 436–440.